CHEMISTRY OF MATERIALS
Article

Chem. Mater. **2010,** *22,* 2341–2346 2341
DOI:10.1021/cm9034769

Spatially Controlled Oxygen Inhibition of Acrylate Photopolymerization as a New Lithography Method for High-Performance Organic Thin-Film Transistors

Jingsheng Shi, Mary B. Chan-Park, Cheng Gong, Hongbin Yang, Ye Gan, and Chang Ming Li*

School of Chemical and Biomedical Engineering, Nanyang Technological University, 70 Nanyang Drive, 637457 Singapore, Singapore

Received November 15, 2009. Revised Manuscript Received January 25, 2010

A new concept-based lithography with use of spatially controlled oxygen inhibition of photopolymerization in acrylate-based materials as a micropatterning technique and its application in high-performance top- and bottom-gated organic thin-film transistors (OTFTs) on flexible substrates are demonstrated. This process does not rely on any surface/interfacial chemistry or adhesives and thus can be used in the patterning of a broad range of materials for printed organic electronics. It is also capable of achieving high resolution (3 μm), which is sufficient in OTFT-based organic electronics applications. The bottom-gated pentacene transistors show a remarkably high mobility of 1.02 cm^2 V^{-1} S^{-1}, which is among the highest mobilities in flexible transistors fabricated by low-cost patterning processes.

Introduction

Organic electronics are the subject of increasing interest for use in low-cost printed electronics on flexible substrates for broad applications such as flexible display, electronic paper, solar panels, and flexible sensors.[1−5] With the performance of organic semiconductors approaching the requirements of the particular applications, the challenge turns to the ability to fabricate the devices at very low cost. This requires not only solution-processable organic semiconductors/dielectrics and cheap flexible substrates but also inexpensive mass manufacturing processes.[4] Photolithography has a long history in the high-performance silicon-based semiconductor electronics industry but is not particularly well-suited for low-end applications like printed electronics because of its requirements for delicate photolithographic tools, expensive photomasks/resists, and intensive labor. Several categories of alternative fabrication processes for printed electronics have been developed, such as microcontact printing (μCP),[6,7] transfer printing,[8−10] inkjet printing,[3,11] etc. μCP is a very powerful patterning technique and has been studied intensively. It has been successfully applied in the fabrication of organic thin-film transistors (OTFTs). The best established system to date for μCP is based on alkanethiolates on gold and silver and alkylsiloxanes on a hydroxyl-terminated surface,[6] in which a specific surface chemistry is required between the ink material and substrate. This requires a specific ink material to be used for the patterning of a certain substrate material, and new inks must be designed accordingly to pattern each new material; this involves significant redesign work and limits the applicability of this patterning technique. In transfer printing, interface chemistry is also necessary when a molecular adhesive is used,[10] and a thick metallic adhesive has been proven to limit the device performance even when conventional patterning techniques are used.[12] Inkjet printing, a convenient patterning method that has been applied in different research areas,[11] is another low-cost fabrication process that has advantages of additive operation, on-demand deposition, and compatibility with flexible and large-area substrates.[13] However, conventional inkjet printing suffers from low-resolution capability and thus is not inadequate for the direct patterning of source and

*To whom correspondence should be addressed. E-mail: ecmli@ntu.edu.sg.

(1) Service, R. F. *Science* **1997**, *278*, 383–384.
(2) Katz, H. E.; Lovinger, A. J.; Johnson, J.; Kloc, C.; Siegrist, T.; Li, W.; Lin, Y. Y.; Dodabalapur, A. *Nature* **2000**, *404*, 478–481.
(3) Sirringhaus, H.; Kawase, T.; Friend, R. H.; Shimoda, T.; Inbasekaran, M.; Wu, W.; Woo, E. P. *Science* **2000**, *290*, 2123–2126.
(4) Forrest, S. R. *Nature* **2004**, *428*, 911–918.
(5) Chabinyc, M. L.; Salleo, A. *Chem. Mater.* **2004**, *16*, 4509–4521.
(6) Xia, Y. N.; Whitesides, G. M. *Annu. Rev. Mater. Sci.* **1998**, *28*, 153–184.
(7) Rogers, J. A.; Zhenan, B.; Anita, M.; Paul, B. *Adv. Mater.* **1999**, *11*, 741–745.
(8) Jingsheng, S.; Chan-Park, M. B.; Li, C. M. *Org. Electron.* **2009**, *10*, 396–401.
(9) Loo, Y.-L.; Willett, R. L.; Baldwin, K. W.; Rogers, J. A. *Appl. Phys. Lett.* **2002**, *81*, 562–564.
(10) Loo, Y.-L.; Willett, R. L.; Baldwin, K. W.; Rogers, J. A. *J. Am. Chem. Soc.* **2002**, *124*, 7654–7655.
(11) Calvert, P. *Chem. Mater.* **2001**, *13*, 3299–3305.
(12) Yoneya, N.; Noda, M.; Hirai, N.; Nomoto, K.; Wada, M.; Kasahara, J. *Appl. Phys. Lett.* **2004**, *85*, 4663–4665.
(13) Menard, E.; Meitl, M. A.; Sun, Y.; Park, J.-U.; Shir, D. J.-L.; Nam, Y.-S.; Jean, S.; Rogers, J. A. *Chem. Rev.* **2007**, *107*, 1117–1160.

Published on Web 02/18/2010

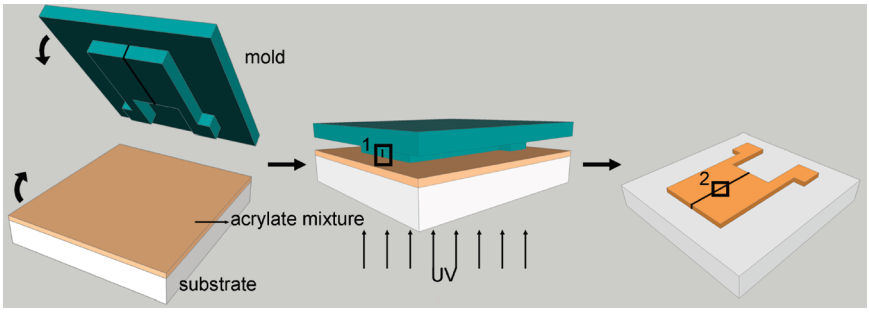

(a)

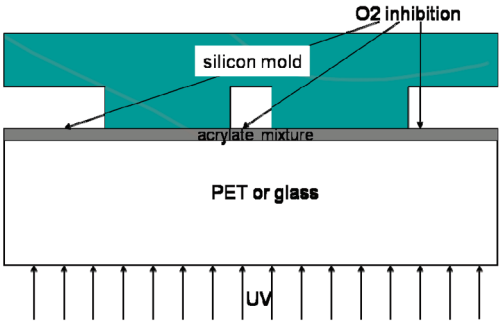

(b)

Figure 1. (a) Schematic illustration of the process to create a pattern on the substrate by spatial control of oxygen inhibition in the photopolymerization of an acrylate-based material to create a polymer mask over metal electrodes in a FET. (b) Schematic illustration (magnified area 1 in part a) of the mechanism of spatially controlled oxygen inhibition.

drain electrodes for OTFTs.[14] The recently reported electrohydrodynamic jet printing approach offers impressive single-micrometer resolution but requires a conductive support to generate an electric field between the nozzle and conductive support, making the process slightly more complicated.[15,16] Thus, there is a great need to develop an economic micropatterning method for printing microelectronics with pattern resolutions on the few micrometer, submicrometer, and nanometer scales.

Here we report a low-cost micropatterning process that employs a reusable silicon mold associated with UV exposure to spatially modulate oxygen inhibition in the UV polymerization process in acrylate-based monomers or oligomers. This is the first demonstration of spatial control of oxygen inhibition in the UV polymerization process and the use of this effect to produce a pattern in an acrylate polymer. The fabrication process does not rely on any surface/interfacial chemistry or additional adhesives and is capable of achieving a high resolution of 3 μm and potentially higher. The fabrication process replaces the elaborate infrastructure of photolithographic tools, photoresists, and photomasks with the simple UV illumination of a low-cost acrylate-based material as a "resist" in contact with a reusable silicon mold, making itself well-suited in low-end applications of printed organic electronics, and we apply it here to the creation of etch masks for the electrodes of top- and bottom-gated OTFTs. The process and its mechanism are illustrated in Figure 1. It is worth noting that it is difficult for a rigid silicon mold to have conformal contact with a hard substrate, thus limiting this process from being applicable to large-area hard substrates.

There are three stages of reactions in an acrylate-based, free-radical polymerization process: initiation, polymerization, and termination. The overall reaction scheme may be represented by the following equations:[17]

Initiation

$$\text{initiator} \xrightarrow{h\nu} \text{R}^{\bullet} \quad (1)$$

Polymerization

$$\text{R}^{\bullet} + \text{M} \rightarrow \text{RM}^{\bullet} \quad (2)$$

$$\text{RM}_n^{\bullet} + \text{M} \rightarrow \text{RM}_{n+1}^{\bullet} \quad (3)$$

Termination

$$\text{RM}_n^{\bullet} + \text{RM}_m^{\bullet} \rightarrow \text{RM}_{m+n} \quad (4)$$

The oxygen inhibition effect occurs through the scavenging of free radicals by oxygen molecules to form oxidized radicals, which are ineffective in the polymerization process. The difference between reaction processes on contacted and uncontacted regions with dissolved oxygen

(14) Bao, Z.; Rogers, J. A.; Katz, H. E. *J. Mater. Chem.* **1999**, *9*, 1895–1904.
(15) Park, J.-U.; Hardy, M.; Kang, S. J.; Barton, K.; Adair, K.; Mukhopadhyay, D. k.; Lee, C. Y.; Strano, M. S.; Alleyne, A. G.; Georgiadis, J. G.; Ferreira, P. M.; Rogers, J. A. *Nat. Mater.* **2007**, *6*, 782–789.
(16) Sekitani, T.; Noguchi, Y.; Zschieschang, U.; Klauk, H.; Someya, T. *Proc. Natl. Acad. Sci. U.S.A.* **2008**, *105*, 4976–4980.
(17) Decker, C.; Jenkins, A. D. *Macromolecules* **1985**, *18*, 1241–1244.

in the acrylate mixture under low incident light intensity can be expressed as the diagram (5)

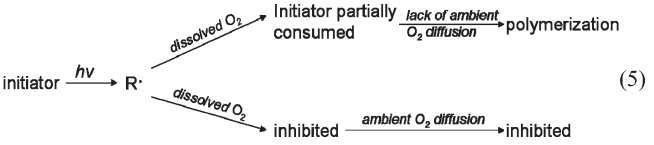

(5)

and the reaction between radicals and oxygen molecules can be further detailed in the following equations:

$$R^{\bullet} + O_2 \rightarrow ROO^{\bullet} \quad (6)$$

$$RM_n^{\bullet} + O_2 \rightarrow RM_nOO^{\bullet} \quad (7)$$

$$ROO^{\bullet} + RM_nOO^{\bullet} \rightarrow \text{termination} \quad (8)$$

where $ROO^{\bullet}$ and $RM_nOO^{\bullet}$ are not capable of initiating the polymerization process.[17]

The oxygen molecules that produce the inhibition effect are provided by dissolved oxygen in the acrylate mixture and diffused ambient oxygen from the depressions of the silicon mold into the acrylate mixture (Figure 1b). Upon UV exposure, as shown in Figure 1b, portions of the acrylate mixture thin film in contact with the silicon mold protrusions are protected from ambient air and would not experience oxygen inhibition after consumption of dissolved oxygen in the acrylate mixture. This would result in photopolymerization of the thin film in contact with the mold, while the uncontacted regions of the thin film would not polymerize. After removal of the silicon mold and the rinsing away of the un-cross-linked acrylate mixture, an acrylate polymer pattern replicating the elevated relief of mold is created on the surface of the substrate.

Experimental Section

Process Details. The detailed process is illustrated in Figure 2a. During fabrication, a mixture of the acrylate monomer and oligomer is spin-coated on a sputtered gold surface on a poly(ethylene terephthalate) (PET) substrate. The mixture is comprised of a monomer (styrene) and an oligomer [ethoxylated bisphenol A diacrylate (SR-349 purchased from Sartomer)] with a ratio of styrene to SR-349 of 1:3 and 0.3 wt % photoinitiator, 2,2-dimethoxy-1,2-diphenylethan-1-one (IRGACURE 651 purchased from Ciba Specialty Chemicals). The low concentration of the photoinitiator was used to maintain a pronounced oxygen-inhibition effect during the polymerization. The molecular structures are shown in Figure 2b. After coating of the gold substrate with the acrylate mixture, the mold is carefully brought into contact with the thin film of the acrylate mixture. UV exposure is applied through the transparent PET substrate and semitransparent gold layer to cross-link the acrylate mixture. After removal of the mold, the un-cross-linked acrylate mixture, which was exposed to oxygen and thus did not cross-link, is removed by soaking of the substrate in isopropyl alcohol (IPA); the cross-linked acrylate polymer remains on the gold surface, forming the desired pattern.

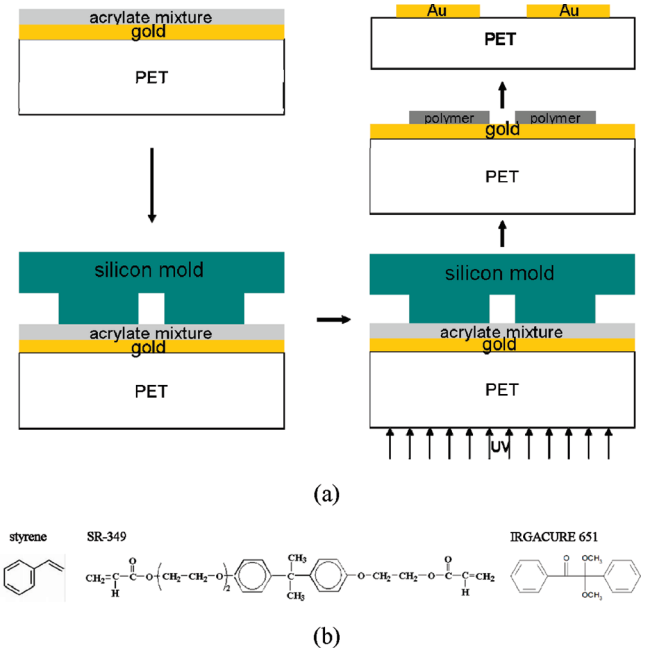

Figure 2. (a) Schematic illustration of polymer mask pattern fabrication on the gold surface and the following gold etching step. (b) Molecular structure of styrene, SR-349, and 2,2-dimethoxy-1,2-diphenylethan-1-one.

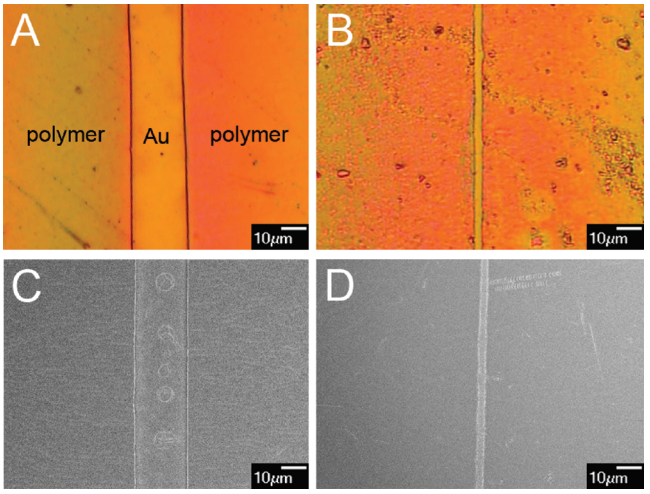

Figure 3. (a) Optical image of the polymer pattern on gold with a resolution of 20 μm at the transistor channel (area 2 in Figure 1). (b) Optical image of the polymer pattern on gold with a resolution of 3 μm. (c) SEM image of the polymer pattern with a resolution of 20 μm. (d) SEM image of the polymer pattern with a resolution of 3 μm.

Silicon Mold. Silicon mold was fabricated by a conventional photolithographic technique followed by a deep reactive-ion-etching dry-etching process. To ensure that the cross-linked polymer pattern does not stick to the mold, the mold was modified with a passivation layer produced by immersion of the mold in a 1 mM solution of 1*H*,1*H*,2*H*,2*H*-perfluorooctyltriethoxysilane in ethanol for 1 h. After creation of the passivation layer, the silicon mold had a very hydrophobic surface with a typical water contact angle of close to 120°. The treated mold is reusable after a simple cleaning by sonication in acetone.

Light Source. UV irradiation was provided by a UV flood cure system (intensity and spectral distribution in the Supporting Information). A gold-coated PET film could filter out

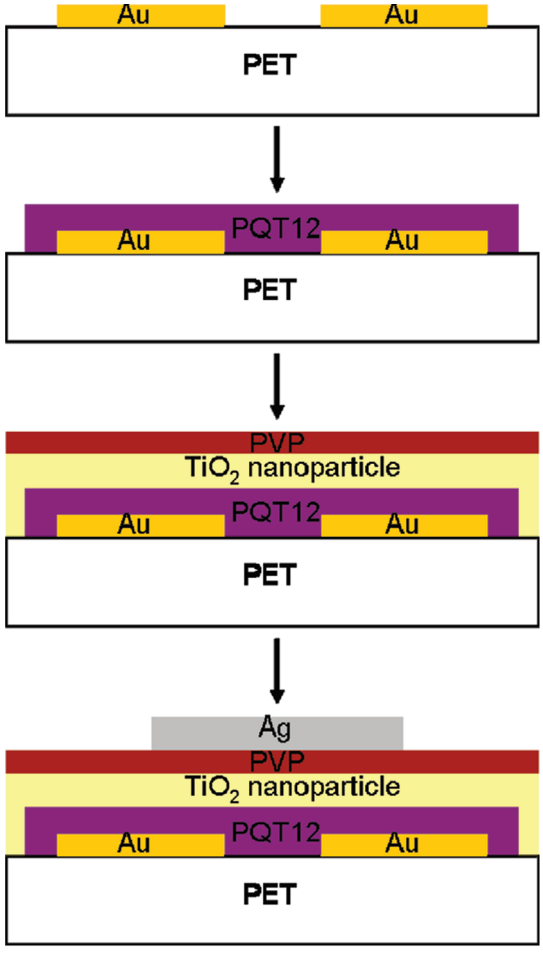

(a)

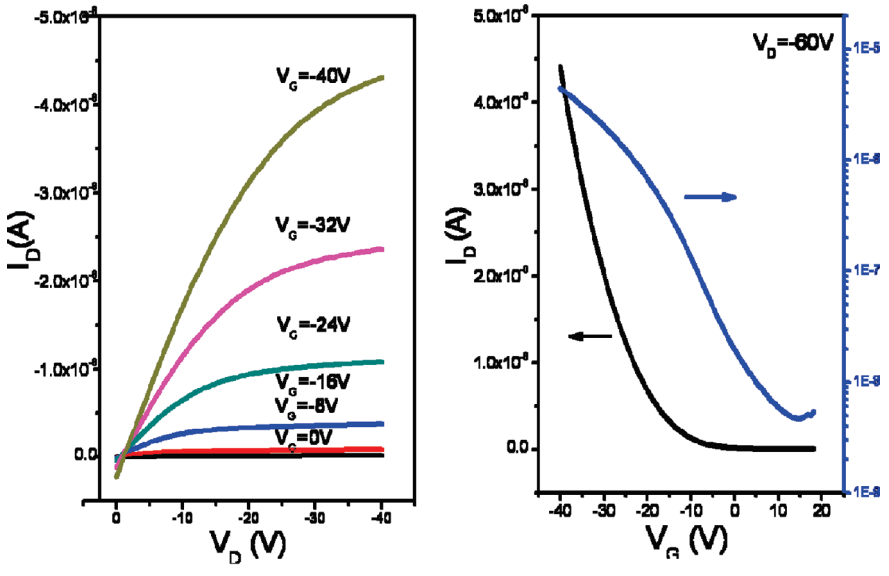

(b)

Figure 4. (a) Fabrication process of a top-gated PQT-12 OTFT. (b) Device performance, as I_D-V_D and I_D-V_G curves, of the fabricated top-gated PQT-12 OTFT.

wavelengths below 310 nm (transmittance in the Supporting Information), resulting in a low effective intensity to avoid suppression of oxygen inhibition at the uncontacted region.

Gold Etching. The unprotected gold was etched away in a solution of KI and I_2 in deionized water ($KI:I_2:H_2O$ = 4:1:100) for 2 min.

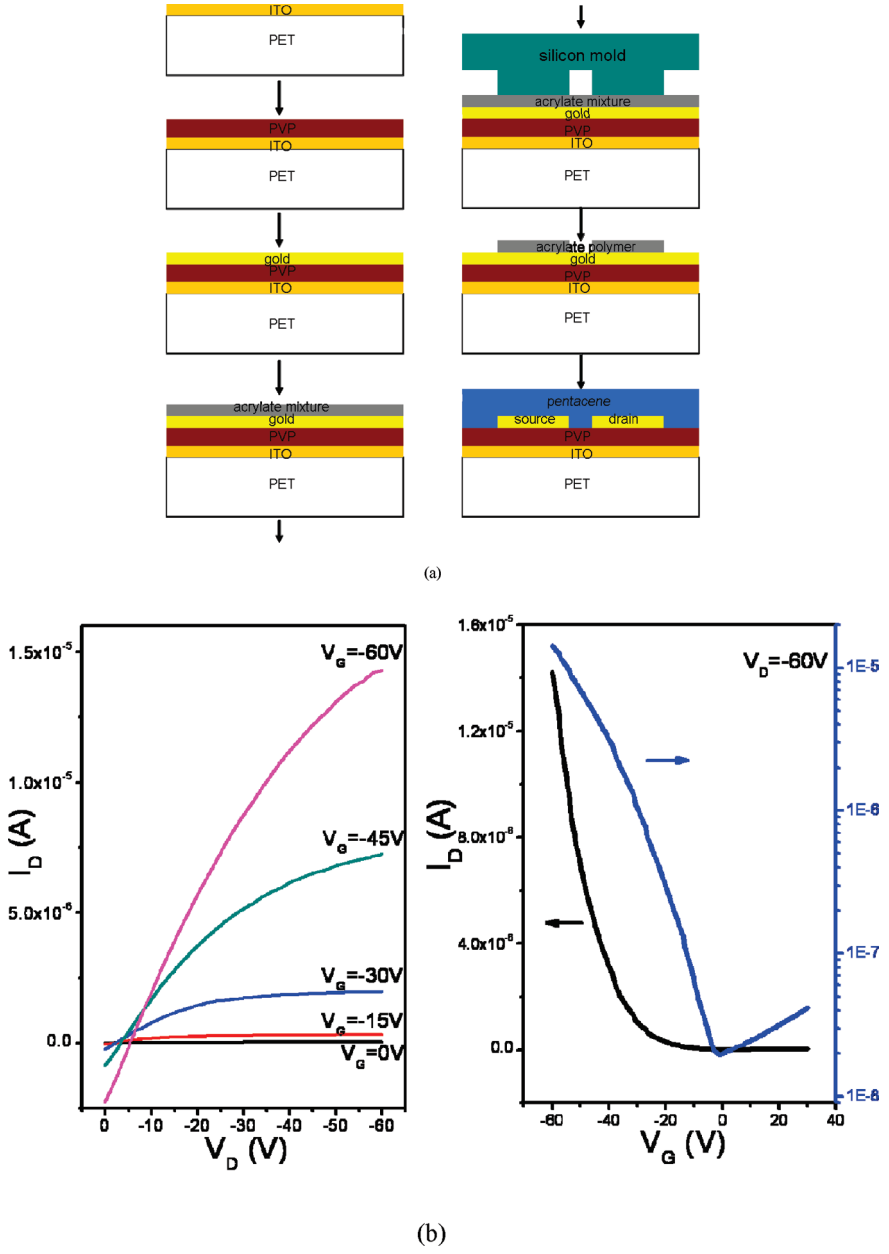

Figure 5. (a) Fabrication process of bottom-gated pentacene OTFT. (b) Device performance, as I_D-V_D and I_D-V_G curves, of the fabricated bottom-gated pentacene OTFT.

Top-Gated PQT-12 Transistor. PQT-12 was dissolved in dichlorobenzene with a concentration of 0.3%, spin-coated at 1000 rpm for 2 min, and annealed in vacuum at 125 °C for 45 min. A TiO_2 nanoparticle solution with a concentration of 35 mg/mL in chlorobenzene was spin-coated at 800 rpm for 1 min. The poly(vinylpyrrolidone) (PVP) solution was 8 wt % PVP in dimethylformamide. The channel dimensions W and L of the PQT-12 transistor were 700 and 20 μm, respectively.

Bottom-Gated Pentacene Transistor. An indium−tin oxide (ITO)-coated PET substrate was purchased from Sigma. The PVP solution was 12 wt % PVP in dimethylformamide. The cross-linking agent for the PVP dielectric was methylated poly(melamine-*co*-formaldehyde). The channel dimensions W and L of the pentacene transistor were 240 and 20 μm, respectively.

Results and Discussion

The region of the polymer pattern formed by this method that would be most critical in the field effect transistor (FET) performance, the area destined to become the active channel after application of a semiconductor material, was characterized by optical microscopy and field-emission scanning electron microscopy (FE-SEM). Figure 3 shows optical (parts a and b) and FE-SEM (parts c and d) images of the acrylate polymer on a gold surface in the area of the transistor channel (area 2 in Figure 1a). Polymer patterns with feature sizes of 20 and 3 μm are shown, demonstrating the relatively high resolution capability (3 μm) of this process.

The microstructure patterned using this new concept of lithography was used to fabricate OTFTs with both bottom- and top-gated configurations. To fabricate top-gated PQT-12 OTFTs, PQT-12 was spin-coated on the gold source and drain electrodes and an active channel gap were produced by etching out the regions of the gold

film not protected by the polymer mask. Solution-processable TiO_2 nanoparticles fabricated in our laboratory were then spin-coated as a primary dielectric material,[18] followed by spin-coating of a PVP solution on the TiO_2 nanoparticle thin film as an additional dielectric material to reduce the gate leakage current. Finally, a 100 nm aluminum gate electrode was deposited by physical vapor deposition, to complete fabrication of the OTFT. The fabrication process is illustrated in Figure 4a. OTFT devices were characterized using an Agilent 4157B Semiconductor Parameter Analyzer System and a probe station in ambient air. The device performance data are shown as I_D-V_D and I_D-V_G curves in Figure 4b. The device mobility in the saturation regime was extracted from the following equation:

$$\mu = \left(\frac{\partial\sqrt{I_D}}{\partial V_G}\right)^2 \frac{2L}{W}\frac{1}{C_i} \quad (9)$$

where I_D is the drain current, C_i is the capacitance per unit area of the gate dielectric layer, and V_G is the gate voltage. The capacitance per unit area of the gate dielectric was separately measured as 4.8 nF cm^{-2}. The field effect mobility, μ, was calculated as 0.06 cm^2 V^{-1} S^{-1}. The device performance is comparable to that of OTFT devices fabricated using photolithographically defined source and drain electrodes.[19]

The bottom-gated transistor configuration requires some adjustments in the fabrication process to put transparent the ITO gate electrode and PVP dielectric under the gold surface. The adjusted process is illustrated in Figure 5a. The ITO-coated PET substrate was cleaned with detergent and deionized water. The PVP solution was spin-coated and cross-linked at 200 °C for 15 min. Gold was then deposited to a thickness of 35 nm using a sputtering system. The acrylate mixture was spin-coated on the gold surface, brought into contact with the mold, and cross-linked with UV exposure to create a mask pattern of the acrylate polymer. After removal of the un-cross-linked acrylate and etching away of the unprotected gold, the cross-linked acrylate polymer mask was removed with acetone, followed by deposition of 65 nm of pentacene using a physical vapor deposition system to complete the OTFT. Although the device structure is different from that of the top-gated transistor, the process only requires an adjustment of the sequence of deposition of the gate electrode, dielectric material, and definition of the source and drain electrodes, while the process for creation of the polymer pattern is the same as that in the fabrication of the top-gated transistor, demonstrating the capability of this process to pattern devices with different structures without modification. After fabrication, the OTFT devices were characterized, and the device performance is shown in Figure 5b. The capacitance per unit area of the gate dielectric was separately measured as 1.7 nF cm^{-2}. The field effect mobility, μ, was calculated as 1.02 cm^2 V^{-1} S^{-1} using eq 9, while the on/off ratio of the transistors was calculated as slightly above 10^3. The transistor performance is adequate for applications such as rectifier circuits of radio-frequency identification tags in lower bands and driver circuits for displays.[20,21] The device performance can be further improved by optimizing the properties of interfaces and contacts in the transistor structures such as the self-assembled monolayer-treated interface and contact reported in our previous work.[22,23]

Conclusion

In conclusion, we have here demonstrated the first use of spatial control of oxygen inhibition of photopolymerization in acrylate-based materials for micropatterning and the use of a micropattern so created as an etch mask in the fabrication of high-performance top- and bottom-gated OTFTs. This method can be employed with solution-processable organic semiconductors and dielectrics and with flexible substrates, providing an innovative and low-cost manufacturing method for OTFT devices. This process does not rely on any surface/interfacial chemistry or adhesives and so can be used in the patterning of a wide range of materials for printed organic electronics without the necessity of idiosyncratic chemistry or surface modifications. It is also capable of achieving high resolution (3 μm), which is sufficient in OTFT applications. The OTFT devices fabricated with this new lithography method demonstrate very good device performance for organic electronics applications. This new approach eliminates the delicate photolithographic tools, expensive photomasks, and resists required by the conventional lithography process, thus providing a much simpler manufacturing process. It may serve as an enabling technology in low-cost medium-performance printed organic electronics.

Acknowledgment. This work was financially supported by the Singapore National Research Foundation under Grant NRF-CRP2-2007-02.

Supporting Information Available: Spectral distribution of incident UV light, incident light intensity distribution at different positions in the UV flood cure system and at different distances from the incident light source, and transmittance of a gold (25 nm)-coated PET film. This material is available free of charge via the Internet at http://pubs.acs.org.

(18) Cai, Q. J.; Gan, Y.; Chan-Park, M. B.; Yang, H. B.; Lu, Z. S.; Song, Q. L.; Li, C. M.; Dong, Z. L. *Appl. Phys. Lett.* **2008**, *93*, 113304-3.
(19) Qin Jia, C.; Ye, G.; Mary, B. C.-P.; Hong Bin, Y.; Zhi Song, L.; Qun Liang, S.; Chang Ming, L.; Zhi Li, D. *Appl. Phys. Lett.* **2008**, *93*, 113304.
(20) Vida, V.; Songs, S.; Kim, J.; Halide, A.; Haddock, J. N.; Kippelen, B.; Wilson, D. M. *IEEE Trans. Circuits Syst. I: Fundam. Theory Appl.* **2008**, *55*, 1177–1184.
(21) Cantatore, E.; Geuns, T. C. T.; Gruijthuijsen, A. F. A.; Gerick, G. H.; Drews, S.; de Leeuw, D. M. *Solid-State Circuits Conf.* **2006**, 1042–1051.
(22) Cai, Q. J.; Chan-Park, M. B.; Lu, Z. S.; Li, C. M.; Ong, B. S. *Langmuir* **2008**, *24*, 11889–11894.
(23) Yuan, G. C.; Xu, Z.; Gong, C.; Cai, Q. J.; Lu, Z. S.; Shi, J. S.; Zhang, F. J.; Zhao, S. L.; Xu, N.; Li, C. M. *Appl. Phys. Lett.* **2009**, *94*, 3.